

Article

Three Vectors Model Predictive Torque Control Without Weighting Factor Based on Electromagnetic Torque Feedback Compensation

Haixia Li ¹, Jican Lin ^{1,*} and Ziguang Lu ²

¹ Department of Mechanical and Control Engineering, Guilin University of Technology, Guilin 541000, China; lihaixia19790604@163.com

² College of Electrical Engineering, Guangxi University, Nanning 530004, China; luziguang@tsinghua.org.cn

* Correspondence: linjican@126.com

Received: 14 March 2019; Accepted: 9 April 2019; Published: 11 April 2019



Abstract: Finite control set-model predictive torque control (FCS-MPTC) depends on the system parameters and the weight coefficients setting. At the same time, since the actual load disturbance is unavoidable, the model parameters are not matched, and there is a torque tracking error. In traditional FCS-MPTC, the outer loop—that is, the speed loop—adopts a classic Proportional Integral (PI) controller, abbreviated as PI-MPTC. The pole placement of the PI controller is usually designed by a plunge-and-test, and it is difficult to achieve optimal dynamic performance and optimal suppression of concentrated disturbances at the same time. Aiming at squirrel cage induction motors, this paper first proposes an outer-loop F-ETFC-MPTC control strategy based on a feed-forward factor for electromagnetic torque feedback compensation (F-ETFC). The electromagnetic torque was imported to the input of the current regulator, which is used as the control input signal of feedback compensation of the speed loop; therefore, the capacity of an anti-load-torque-disturbance of the speed loop was improved. The given speed is quantified by a feed-forward factor into the input of the current regulator, which is used as the feed-forward adjustment control input of the speed controller to improve the dynamic response of the speed loop. The range of the feed-forward factor and feed-back compensation coefficient can be obtained according to the structural analysis of the system, which simplifies the process of parameter design adjustment. At the same time, the multi-objective optimization based on the sorting method replaces the single cost function in traditional control, so that the selection of the voltage vector works without the weight coefficient and can solve complicated calculation problems in traditional control. Finally, according to the relationship between the voltage vector and the switch state, the virtual six groups of three vector voltages can be adjusted in both the direction and amplitude, thereby effectively improving the control performance and reducing the flow rate and torque ripple. The experiment is based on the dSPACE platform, and experimental results verify the feasibility of the proposed F-ETFC-MPTC. Compared with traditional PI-MPTC, the feed-forward factor can effectively improve the stability time of the system by more than 10 percent, electromagnetic torque feedback compensation can improve the anti-load torque disturbance ability of the system by more than 60 percent, and the three-vector voltage method can effectively reduce the disturbance.

Keywords: model predictive torque control; electromagnetic torque feedback compensation; feed-forward factor; weight coefficient; three vectors

1. Introduction

Field-oriented control (FOC) [1] and direct torque control (DTC) [2] has been successfully and widely used because of its robustness and fast response, which qualifies the requirements of high

performance control for Induction Motor (IM) drives. FOC controls the torque and flux by controlling the d-q axis component of the stator current of the motor. DTC controls the torque and flux of the motor directly by the torque and flux hysteresis controller. Based on the two control strategies, the PI controller used in the speed outer loop needs to be tuned. The parameters are affected by the inverter driving the voltage, motor current, and so forth. At the same time, the integral term is included. When a step signal is input, the integral saturation easily occurs, which leads to the overshoot of the control system and delays the stability time of the system. In order to improve the control effect of the outer loop, a variety of control strategies have been proposed. Reference [3] validates that the Integral Proportional (IP) speed controller could reduce the overshoot of the system to a certain extent, but that it has insufficient setting efficiency and tracking response. According to Reference [4], the IP controller was used in the speed control of a permanent magnet synchronous motor, and the electromagnetic torque was used as the feedback compensation of the IP speed controller to improve the anti-disturbance ability of the load.

With the increasing complexity of multi-phase motor systems and the development of microprocessors, more and more attention has been paid to Model Predictive Control (MPC) [5,6], which is mainly based on the calculation of future system behavior to calculate the optimal execution variables. MPC can be divided into continuous control set-model predictive control (CCS-MPC) [7] and finite control set-model predictive control (FCS-MPC) [8]. In the motor drive system, according to the different control objectives, the finite control set model predictive control method can be divided into Model Predictive Current Control (MPCC) [9,10] and Model Predictive Torque Control (MPTC) [11]. MPTC takes stator flux and electromagnetic torque as control objectives. In order to balance the influence of the two control variables on the system, weight coefficients are usually designed to adjust the proportion of the two control variables in the cost function. The weight coefficient design is mostly experimentation through the empirical method, and the process is rather complicated. In [12], an online optimization of weighting coefficients for induction motors was proposed. The weighting coefficients were optimized by minimizing torque ripple, but the problem of computation was not solved yet. In [13], by investigating the relationship between torque, the reference stator flux amplitude, and the phase angle of the stator flux, the reference stator flux vector was constructed. The cost function contains only the stator flux vector, and the calculation of the weight coefficient was omitted. A cost function containing only a reference voltage tracking error was designed to eliminate the weighting factor in [14].

The traditional MPTC has only one voltage vector working during a period, which resulted in large torque and flux ripple. In order to improve the steady-state performance of the system, common methods include increasing the number of alternative vectors [15,16], adjusting the amplitude of voltage vectors [17], and expanding the direction of voltage vectors [18,19]. In the method of vector-alternative optimization, the method of synthesizing one virtual voltage vector from two adjacent effective voltages in eight vectors and six sectors had 12 alternative voltage vectors overlapping with the six basic voltage vectors in [15]. Although the voltage vector has increased, the effect of system improvement is not obvious. In [16], six virtual voltage vectors were added and one zero voltage vector was added [15], totaling to 19 optional voltage vectors. However, the cycle needed to be optimized ten times to increase the amount of computation. Another study proposed a three-vector scheme to reduce torque and flux ripple, but the first voltage vector, which applied to the next control cycle, was limited to the last voltage applied in the previous cycle [20].

In order to improve the ability of PI-MPTC to resist the disturbance of load torque and to solve the optimization problem of weight coefficient and voltage vector selection in a squirrel cage induction motor, this paper presents a three-vector model predictive torque control based on electromagnetic torque feedback compensation. In this method, the feed-forward factor is added to the IP controller, and combined with the strong response ability of the PI controller, the control effect of the system is improved, and the real-time electromagnetic torque feedback is applied to the control compensation of the controller. The steady-state performance and anti-load disturbance ability of the system are effectively improved. At the same time, an online sorting method is used to select voltage vectors.

The cost function is to sort the voltage vectors according to the errors of torque and flux in a cycle, as well as to select the optimal voltage vectors, so that the correct operation does not need weight coefficients. Finally, three voltage vectors are applied in each control period, including two active voltage vectors and one zero-voltage vector. The control strategy is intuitive and easy to implement due to the three vectors applied being adjacent. The experimental results prove that the proposed method can effectively reduce torque and flux ripple, speed up the dynamic response, and improve the ability to resist load torque disturbance.

2. Mathematical Model of Induction Motor

The IM state space model in the synchronous reference frame is [20]:

$$\vec{u}_s = R_s \vec{i}_s + \frac{d\vec{\Psi}_s}{dt} \quad (1)$$

$$0 = R_r \vec{i}_r + \frac{d\vec{\Psi}_r}{dt} - j\omega_r \vec{\Psi}_r \quad (2)$$

$$\vec{\Psi}_s = L_s \vec{i}_s + L_m \vec{i}_r \quad (3)$$

$$\vec{\Psi}_r = L_m \vec{i}_s + L_r \vec{i}_r \quad (4)$$

$$T_e = \frac{3}{2} n_p \left\{ \vec{\Psi}_s \otimes \vec{i}_s \right\} \quad (5)$$

where \vec{u}_s and \vec{i}_s are the stator voltage and current vector, $\vec{\Psi}_s$ and $\vec{\Psi}_r$ are the flux vectors of stator and rotor, L_m is the inductance between the stator and rotor, $L_{r/s}$ is the rotor/stator self-inductance, $R_{r/s}$ is the rotor/stator resistance, ω_r is the rotor electrical angular velocity, T_e is the electromagnetic torque, n_p is the number of motor pole-pairs, and \otimes is the outer product (cross product, vector product) operator.

According to the above formula, the stator current can be described as follows:

$$\vec{i}_s = -\frac{1}{R_\sigma} \left(\left(L_\sigma \cdot \frac{d\vec{i}_s}{dt} - k_r \left(\frac{1}{T_r} - j \cdot \omega_r \right) \cdot \vec{\Psi}_r \right) - \vec{u}_s \right) \quad (6)$$

where $R_\sigma = R_s + k_r^2 R_r$, $L_\sigma = \sigma L_s$, $k_r = L_m / L_r$, $\sigma = 1 - L_m^2 / L_s L_r$ and $T_r = L_r / R_r$. According to the forward Euler formula $\frac{dx}{dt} \approx \frac{[x((k+1)T_s) - x(kT_s)]}{T_s}$, the formula (1) and (6) can be discretized as follows:

$$\begin{cases} \vec{\Psi}_s(k+1) = \vec{\Psi}_s(k) + T_s \cdot \vec{u}_s(k) - R_s T_s \cdot \vec{i}_s(k) \\ \vec{i}_s(k+1) = \left(1 - \frac{T_s}{\tau_\sigma} \right) \cdot \vec{i}_s(k) + \\ \frac{T_s}{\tau_\sigma} \frac{1}{R_\sigma} \left[\left(\frac{k_r}{T_r} - k_r j \cdot \omega_r(k) \right) \cdot \vec{\Psi}_r(k) + \vec{u}_s(k) \right] \end{cases} \quad (7)$$

In the equation $\tau_\sigma = L_\sigma / R_\sigma$, T_s is the sampling time and $\vec{u}_s(k)$ is the applied voltage vector. According to formula (7), the flux and the electromagnetic torque at the $(k+1)$ th instant can be calculated:

$$\vec{\Psi}_r(k+1) = \frac{L_r}{L_m} \vec{\Psi}_s(k+1) + \vec{i}_s(k+1) \left(L_m - \frac{L_r L_s}{L_m} \right) \quad (8)$$

$$T_e(k+1) = \frac{3}{2} n_p \left(\vec{\Psi}_s(k+1) \otimes \vec{i}_s(k+1) \right) \quad (9)$$

3. Feed-Forward Factor-Based Electromagnetic Torque Feedback Compensation (ETFC) Controller Analysis

3.1. Analysis of Speed Closed-Loop PI Controller

In the IM system, the torque difference on the motor shaft can be simplified as an integral link after the Laplace transformation has been obtained:

$$\omega_r = \frac{T}{Js} \quad (10)$$

where J is the moment of inertia, and $T = T_e - T_L$, T_L is the motor load torque. Based on the closed-loop control of rotational speed, because of the existence of filtering in both the torque feedback and torque setting, we can make it equivalent to an inertial link. According to the expression of electromagnetic torque $T_e = \frac{n_p L_m}{L_r} i_{st} \psi_r$, it can be simplified as:

$$K_T = \frac{n_p L_m}{L_r} \psi_r \quad (11)$$

The speed loop structure of the induction motor speed control system is shown in Figure 1:

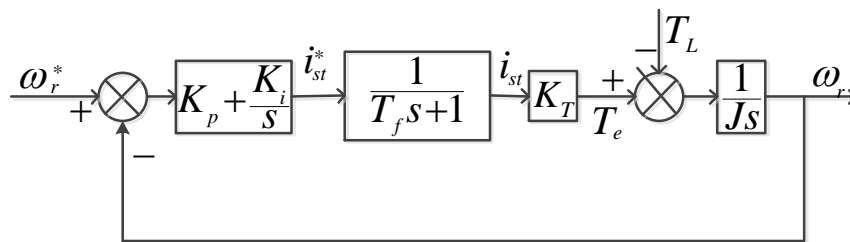


Figure 1. PI control of the induction motor speed loop.

Where ω_r^* is the speed setting, i_{st}^* is the torque current setting, i_{st} is the armature current which is proportional to torque, and T_f is the time constant, which is the delay time of the Pulse Width Modulation (PWM) device. According to Figure 1, suppose the current loop is completely tracked, where $G(s) = \frac{1}{T_f s + 1} = 1$. The transfer functions of the controllers can be obtained, respectively, as follows:

$$G_T(s) = \frac{\omega_r}{T_L} = -\frac{s}{Js^2 + K_T K_{ps} + K_T K_i} \quad (12)$$

$$G_\omega(s) = \frac{\omega_r}{\omega_r^*} = \frac{K_T K_{ps} + K_T K_i}{Js^2 + K_T K_{ps} + K_T K_i} \quad (13)$$

Formulas (12) and (13) show that $G_T(s)$ and $G_\omega(s)$ cannot be set independently. If the load intervention changes sharply, the speed is prone to fluctuation. It can also be seen in (13) that the molecular differential term in the transfer function is large, so the given speed signal is a step signal, which is likely to cause speed overshoot and current instability.

3.2. Analysis of Speed Closed-Loop IP Controller

In order to reduce the influence of the parameter differential term in the speed loop, a proportional link is added into the feedback channel to obtain the IP controller. The structure diagram is shown in Figure 2.

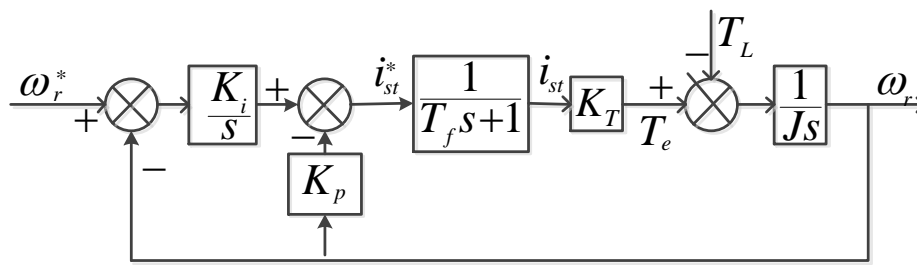


Figure 2. IP control of induction motor speed loop.

Assuming that the current loop is fully tracked, the two transfer functions in the controller are, respectively:

$$G_T(s) = \frac{\omega_r}{T_L} = -\frac{s}{Js^2 + K_T K_P s + K_T K_i} \tag{14}$$

$$G_\omega(s) = \frac{\omega_r}{\omega_r^*} = \frac{K_T K_i}{Js^2 + K_T K_P s + K_T K_i} \tag{15}$$

Analyses (13) and (15) show that the PI and IP controllers have the same characteristic equation, and the transfer function of IP controllers did not have $K_T K_P s$. Therefore, when the given value is the same step signal, IP controllers can effectively reduce the overshoot of the speed loop and the impulse current of the excitation current.

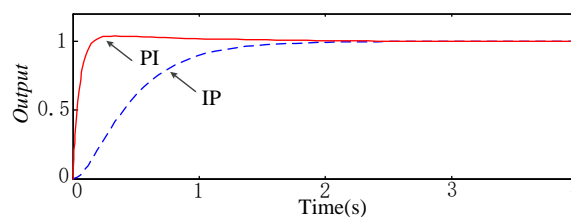
For analyses (12) and (14), IP speed controllers and PI speed controllers have the same transfer functions for speed changes caused by load torque disturbances, so the two speed controllers have the same ability to resist load torque disturbances under the same PI parameters.

In order to further analyze the performance of the two controllers, the given value $\psi_r^* = 0.25$. The motor parameters in Table 1 add to (13) and (15), given $K_P = K_i = 1$, the analysis system step response, and bode diagram.

The analysis Figure 3 shows that the IP controller has a smaller overshoot than the PI controller, and the impulse current of the excitation current component is restrained to some extent. However, the IP controller has larger phase lag, an insufficient tracking response, and a slower response than the PI controller.

Table 1. IM parameters.

Parameter	Symbol	Value
Rotor inductance	L_r	0.4034 H
Mutual inductance	L_m	0.395 H
Stator inductance	L_s	0.4043 H
Rotor resistance	R_r	2.444 Ω
Stator resistance	R_s	3.4 Ω
Number of pole pairs	n_p	2
Moment of Inertia	J	0.005 kg · m ²



(a)

Figure 3. Cont.

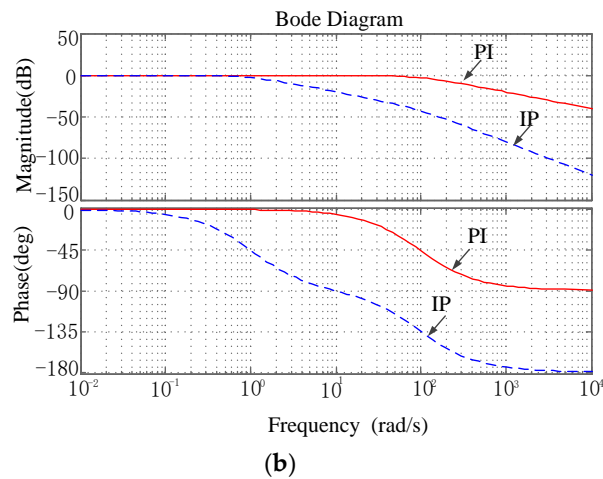


Figure 3. Speed system (comparison between PI and IP controller): (a) unit step response; (b) system bode diagram.

3.3. Feedforward Factor-Based Electromagnetic Torque Feedback Compensation (F-ETFC) Controller

From the above analysis, it can be concluded that the IP controller has an insufficient tracking response, the PI controller is prone to overshoot, and the anti-load torque disturbance ability of the two control systems is the same. For this reason, the feed-forward factor and electromagnetic torque compensation are added to the IP controller, and the structure of the feed-forward factor based electromagnetic torque feedback compensation is shown in Figure 4, which will be referred to as F-ETFC in the following text.

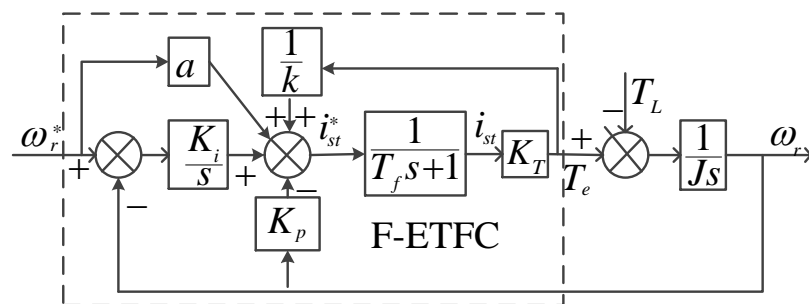


Figure 4. Feedforward Factor-Based Electromagnetic Torque Feedback Compensation (F-ETFC) control of induction motor speed loop.

$$G_T(s) = \frac{\omega_r}{T_L} = -\frac{s(1 - K_T/k)}{(1 - K_T/k)Js^2 + K_TK_p s + K_TK_i} \tag{16}$$

$$G_\omega(s) = \frac{\omega_r}{\omega_r^*} = \frac{\alpha K_T s + K_T K_i}{(1 - K_T/k)Js^2 + K_T K_p s + K_T K_i} \tag{17}$$

An analysis of Figure 4 shows that when the transfer function is without feedback compensation where $1/k$ does not exist, the system is an IP controller when $\alpha = 0$ and a PI controller when $\alpha = K_p$. In order to better combine the advantages of the two controllers, the range of feedforward factor K is defined as $[0, K_p]$. The characteristic equation in transfer function (16) and (17) can be calculated:

$$(1 - K_T/k)Js^2 + K_TK_p s + K_TK_i = 0 \tag{18}$$

In order to make the system stable, we can obtain it based on the Routh criterion.

$$k > K_T \tag{19}$$

- The impact of k changes on the system:

In order to analyze the effect of k changes on the system, the system changes under the conditions of $k = 2K_T$, $k = 5K_T$, and $k = 10K_T$ were analyzed by substituting the values in (16) and (17) in Table 1, and we also considered that parameter tuning could not be carried out simultaneously, thereby taking $\alpha = K_P = K_i = 1$.

As shown in Figures 5 and 6, when the real-time electromagnetic torque feedback is used as the compensation increment of the IP controller, the anti-load torque disturbance ability of the system can be effectively improved when the values of k and K_T are similar, while the value of k has little effect on the dynamic response performance of the speed loop.

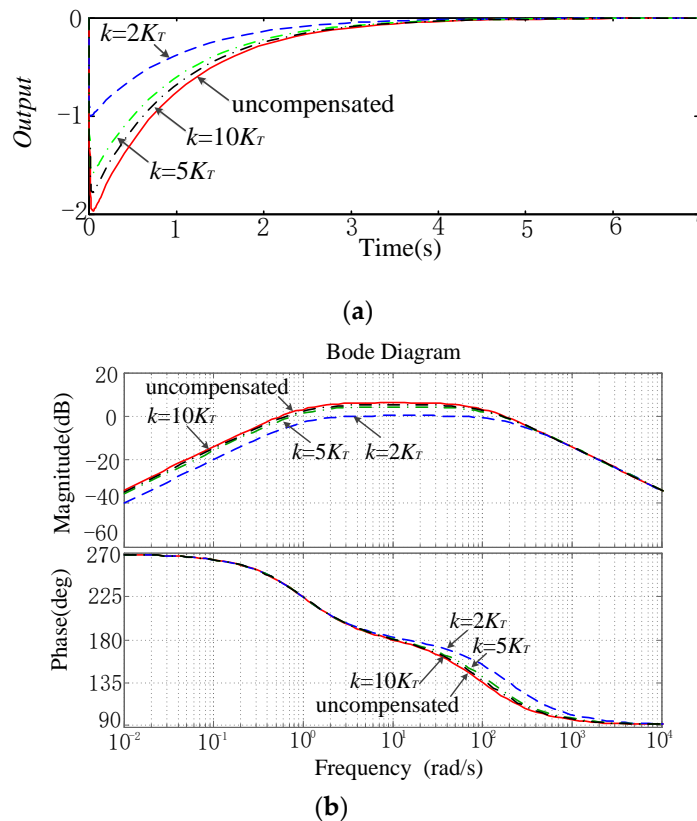


Figure 5. System change of load torque system with k changing. (a) Response characteristics of step torque disturbance of load; (b) Bode diagram of load torque system.

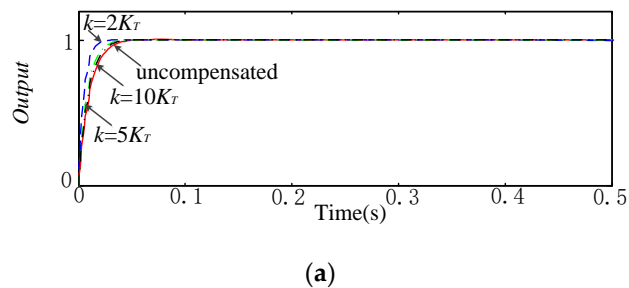


Figure 6. Cont.

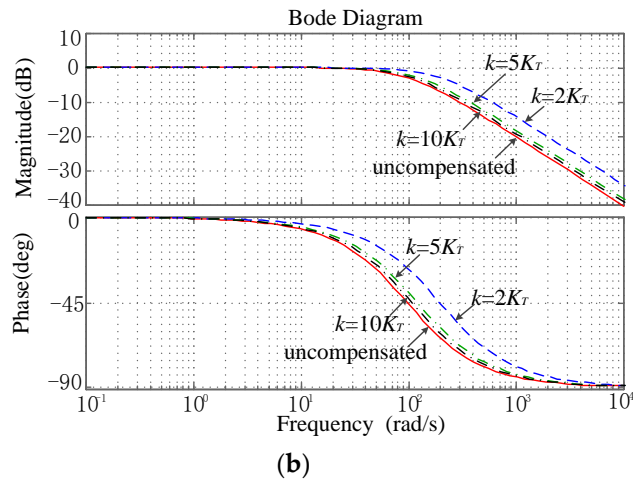


Figure 6. System change of speed system with k changing. (a) Response curve of speed step input; (b) Bode diagram of speed system.

- The impact of α changes on the system:

Here, the influence of α changes on the dynamic response performance of a F-ETFC speed loop is verified. The system changes of Equation (10) in $\alpha = 1, \alpha = 3, \alpha = 6, \alpha = 9$ are analyzed by taking $K_P = 10, K_i = 1, k = 2K_T$.

From the analysis in Figure 7, we can see that the change of α has a great influence on the speed loop of the system in the F-ETFC speed controller. When the value of α is closer to the value of K_P , the stability time of the system can be effectively improved.

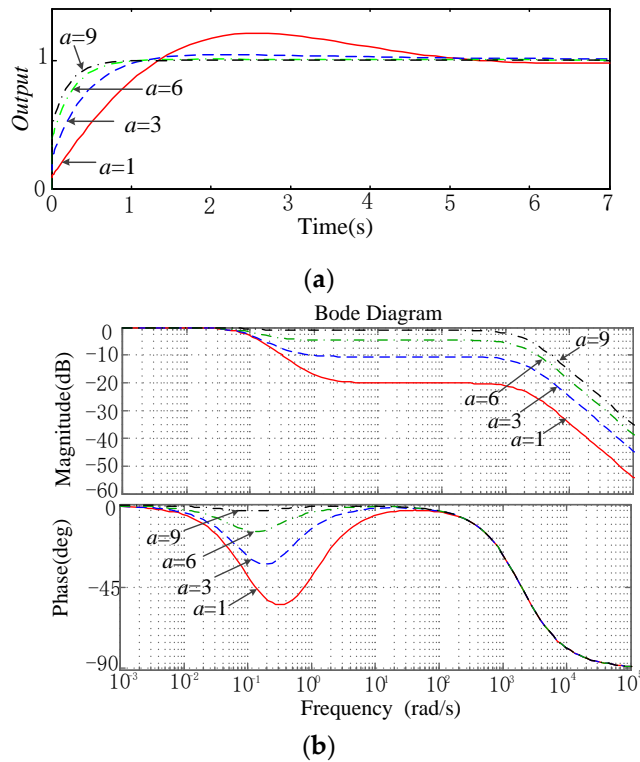


Figure 7. System change of speed system with α changing. (a) Response curve of speed step input; (b) Bode diagram of speed system.

The mechanical constant of the rotor is much larger than the sampling time, so $\omega_r(k) = \omega_r(k+1)$ can approximately be obtained. When the minimum cost function in (21) is selected, the stator voltage vector obtained can be applied to the next sampling time.

4.3. Multi-Objective Ranking

The problem of target optimization in each sampling period in MPTC can be expressed as two different cost functions, where g_1 and g_2 are the errors related to the torque and stator flux, respectively. The proposed strategy based on multi-objective sorting evaluates the sorting for each possible voltage vector of the converter, and references for analytical methods can be found here [21].

$$g_1 = |T_e^* - |T_e(k+2)|| \quad (25)$$

$$g_2 = \left| \psi_s^* - \left| \vec{\psi}_s(k+2) \right| \right| \quad (26)$$

First, sort the values obtained from the evaluation of each objective function g_1 and g_2 . Then, assign a ranking value to each error value. Voltage vectors with lower errors are assigned lower ranks, while voltage vectors with higher errors are assigned higher ranks. That is:

$$g_1(\vec{u}_s(k+1)) \rightarrow r_1(\vec{u}_s(k+1)) \quad (27)$$

$$g_2(\vec{u}_s(k+1)) \rightarrow r_2(\vec{u}_s(k+1)) \quad (28)$$

where $\vec{u}_s(k+1)$ are the evaluated voltage vectors and $r_1(\vec{u}_s(k+1))$ and $r_2(\vec{u}_s(k+1))$ are the ranking values related to g_1 and g_2 .

The ranking value determines the relative quality of each possible voltage vector relative to all remaining possibilities. By selecting a ranking with a minimum value, the optimal voltage vector can be selected from the perspective of a variable error, such as torque error and flux error. In order to determine which are the best total voltage vectors among these alternatives, the average standard is used, in which the voltage vector with the lowest ranked average is selected, resulting in the same compromise for tracking the two variables, torque and flux. Finally, an optimization scheme based on average ranking is proposed.

$$u_{opt} = \arg \min_{\{v0, \dots, v7\}} \frac{r_1(\vec{u}_s(k+1)) + r_2(\vec{u}_s(k+1))}{2} \quad (29)$$

The optimization proposed in (29) can be simplified to the sum of r_1 and r_2 because the optimization problem is equivalent.

4.4. Three-Vector Optimization Principle

In order to achieve a better steady-state performance and reduce torque and flux ripple, a three-vector control strategy is proposed. This strategy virtualizes six alternative voltage vectors online, rather than the traditional eight basic voltage vectors, and the effective range system control is expanded effectively. The alternative voltage vector is synthesized by three adjacent voltage vectors, as shown in Figure 9.

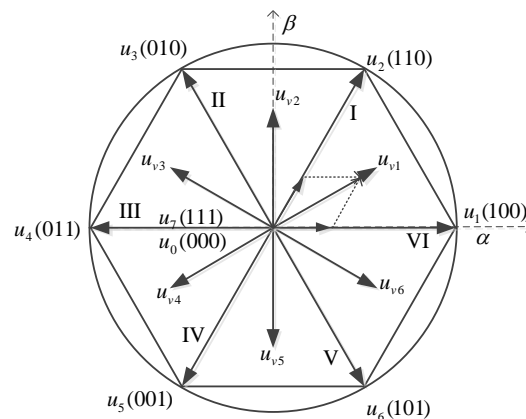


Figure 9. Voltage vector chart.

In Figure 9, u_0 – u_7 are eight basic voltage vectors, and u_{v1} – u_{v6} are six virtual voltage vectors, where u_{v1} is synthesized by the two components $\frac{t_1}{T_s}u_1$ and $\frac{t_2}{T_s}u_2$, and t_1 and t_2 are the optimal duration of the first voltage vector u_{opt1} and the second voltage vector u_{opt2} . Assuming that t_0 is the optimal time for the zero-voltage vector, the vector output selected is:

$$u_{opt} = \frac{t_1}{T_s}u_{opt1} + \frac{t_2}{T_s}u_{opt2} + \frac{t_0}{T_s}u_{opt0} \quad (30)$$

According to the sine rule of the angle included between u_{v1} and u_1 , the state retention time of each vector can be obtained as follows:

$$T_s = t_1 + t_2 + t_0 \quad (31)$$

It can be seen from Figure 9 that the single-vector MPC provides the most limited voltage vector, and only one of the eight basic voltage vectors with a fixed direction and amplitude can be selected. In the duty ratio method, the zero vector and effective vector can be adopted to adjust the magnitude of the expected voltage vector, but their direction is still fixed. The double-vector method extended can not only adjust the direction of the expected voltage vector, but also change the magnitude of the expected voltage vector. The three-vector method proposed constructs six groups of candidate voltage vectors with adjustable amplitude and direction, which covers the entire vector selection area and expands the feasible range of MPC. Based on the above analysis, the new policy schematic presented in this paper is shown in Figure 10.

Based on the above principles, the experimental results can be assumed as follows:

(1) The voltage selection strategy of multi-objective sorting can replace the cost function with weight coefficients.

(2) The optimization of three-vector voltage can effectively reduce the fluctuation of flux and torque than single-vector voltage selection.

(3) Compared with PI control strategy, F-ETFC control strategy can effectively improve the system's resistance to load torque disturbance and improve the system's dynamic response.

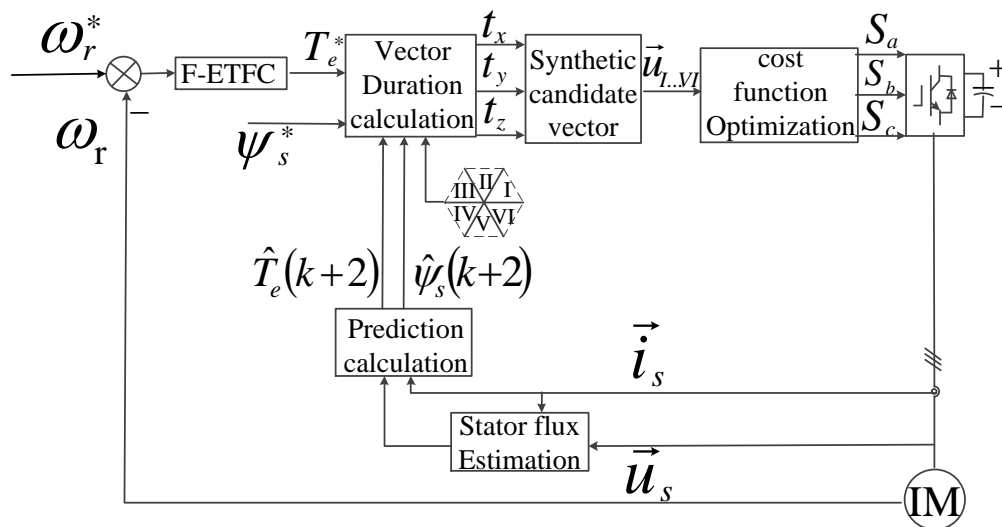


Figure 10. Feedforward Factor-Based Electromagnetic Torque Feedback Compensation-Model Predictive Torque Control (F-ETFC-MPTC) control schematic diagram.

5. Experimental Results

To verify the feasibility of the three-vector voltage optimization current predictive control proposed in this paper in induction motor, the “back-to-back” converter experimental platform was constructed based on DS1104 of dSPACE platform. The photographic view shown in Figure 11 depicts the universal experimental platform. The motor parameters were shown in Table 1. To distinguish the control strategy, the traditional single-vector PI-MPTC method is PI-MPTC-I, the three-vector PI-MPTC method is PI-MPTC-II, and the three-vectors model predictive torque control without a weighting factor based on electromagnetic torque feedback compensation proposed in this paper is F-ETFC-MPTC.

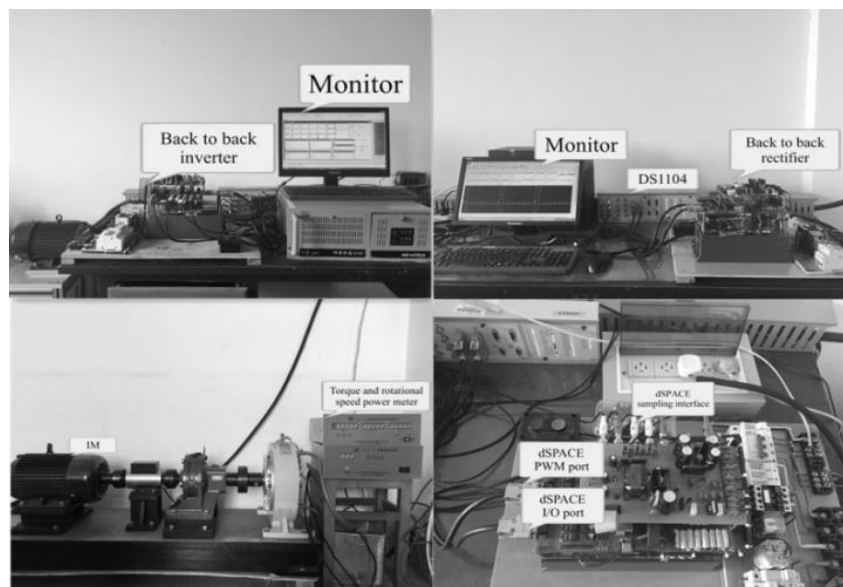


Figure 11. Experimental platform.

The other data of the motor are as follows: rated power (2.2 kW), rated voltage (380 V), rated speed (1422 rpm), rated frequency (50 Hz), stator leakage inductance (9.5 mH), rotor leakage inductance (8.4 mH), and magnetizing inductance (0.2629 H).

The sampling frequency of PI-MPTC-I is set to 10 kHz, while the sampling frequency of both PI-MPTC-II and F-ETFC-MPTC is 8 kHz to show its superiority.

From top to bottom, the curves shown in Figure 12 are steady-state waveforms of speed, torque, stator flux, and stator current, with different weights at a given speed of 400 r/min. Obviously, when the weight coefficient $k_{\psi T}$ is set to 5, although the torque ripple is relatively small, there are obvious pulsations in the flux and current. When $k_{\psi T}$ is increased from 5 to 50, the stator flux linkage and torque ripple are well-balanced. When $k_{\psi T}$ is further increased to 100, the flux ripple changes very little, but the torque ripple and stator current harmonics increase significantly, affecting the stable operation of the speed loop. At the last $k_{\psi T} = 200$, the speed is almost zero, seriously affecting the operation of the system. The results show that, in order to make the torque and stator flux in PI-MPTC have better steady-state characteristics and to make a better comparison between the proposed strategies, for the experimental IM, after much experimental debugging, $k_{\psi T} = 40$ is a suitable solution for PI-MPTC with a weight coefficient.

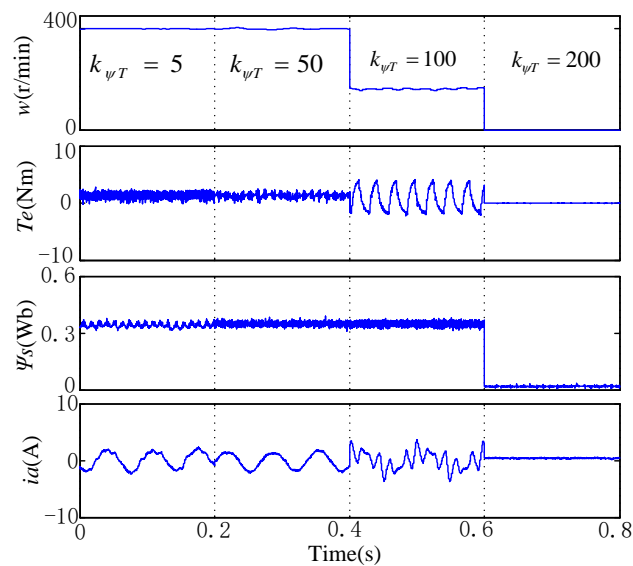


Figure 12. Experimental results of steady-state performance of PI-MPTC-I under different weighting factors.

- A. Step Speed Transient Characteristic

The dynamic characteristics of the three-vector PI-MPTC-II were analyzed and compared with the traditional single-vector PI-MPTC-I. The motor starts at 200 r/min and then suddenly speeds up to 400 r/min. Both methods can track a given speed quickly and accurately, and both methods have the same speed rise time, as shown in Figure 13.

Experimental results of PI-MPTC with different vector selection are shown in Figure 14. The stator flux is almost constant in the process, and the flux and torque can be decoupled. Moreover, PI-MPTC-II has the same dynamic response as PI-MPTC-I, as well as very close steady-state characteristics. However, the flux and torque ripple of PI-MPTC-II is smaller than that of PI-MPTC-I, so the three-vector voltage vector can effectively reduce the torque and flux ripple.

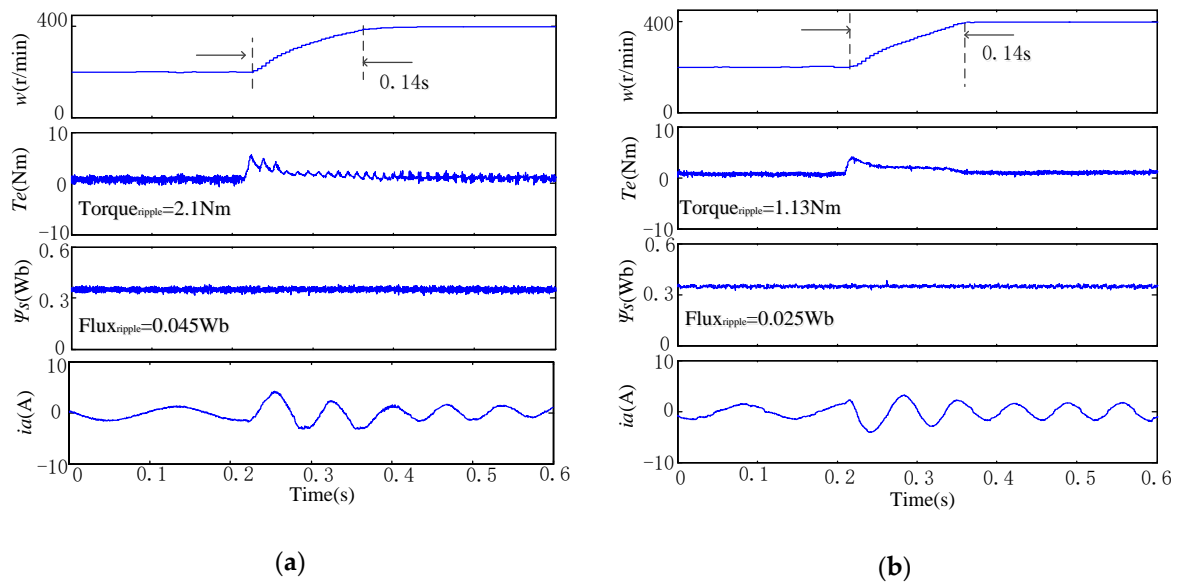


Figure 13. Experimental step speed responses: (a) PI-MPTC-I, (b) PI-MPTC-II.

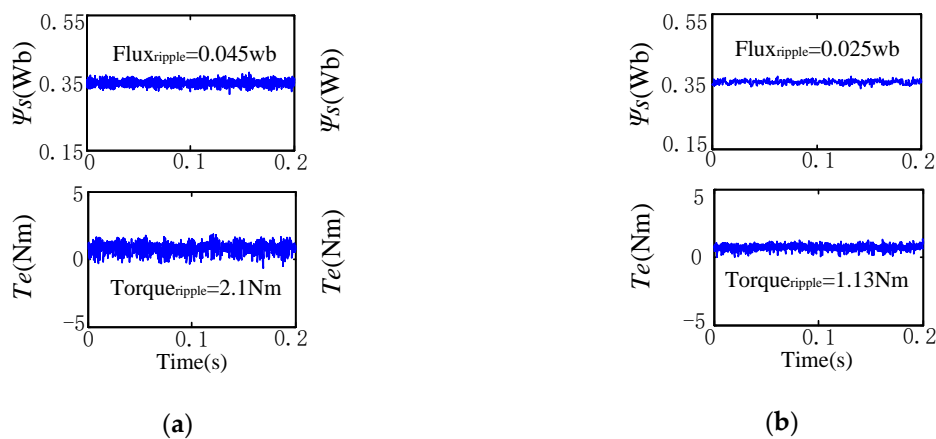


Figure 14. Experiment results of (a) PI-MPTC-I, (b) PI-MPTC-II.

The dynamic characteristics of the three-vector F-ETFC-MPTC were analyzed and compared with the three-vector PI-MPTC-II. The two controller parameters were shown in Table 2, and the experimental results were shown in Figure 15. A comparison of flux and torque ripple between the two control strategies is shown in Figure 16.

Table 2. Parameters of two controllers.

PI-MPTC-II Control Parameters		F-ETFC-MPTC Control Parameters	
ψ_s^*	0.35	ψ_s^*	0.35
K_{p_w}	0.5	K_{p_w}	0.5
K_{i_w}	0.2	K_{i_w}	0.2
		k	$1.5K_T$
		α	0.5

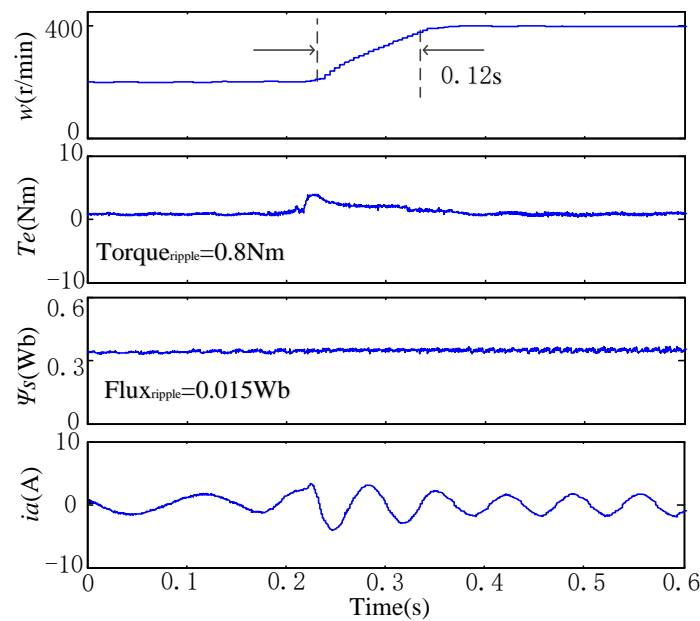


Figure 15. Experimental step speed responses of F-ETFC-MPTC.

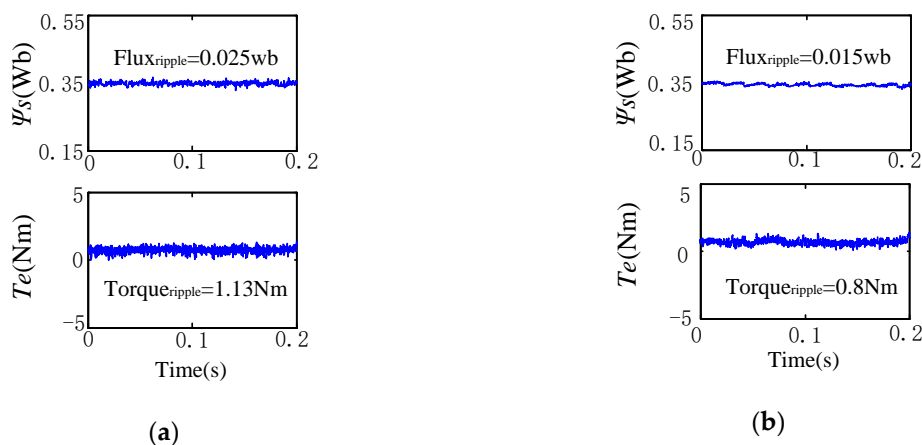


Figure 16. Experimental results: (a) PI-MPTC-II, (b) F-ETFC-MPTC.

From Figure 15, the dynamic response of F-ETFC-MPTC is better than that of PI-MPTC-II. The feed-forward factor is added to improve the steady-state time of the system, and the dynamic response time of the speed loop is increased by about 14%. It can be observed that the F-ETFC-MPTC shows much lower torque and flux ripples compared to PI-MPTC-II in Figure 16. Besides, F-ETFC-MPTC does not need weight coefficient adjustment. It is verified that the voltage selection strategy of multi-objective sorting can replace the cost function with weight coefficients. Based on the results, compared with the traditional MPTC, the proposed F-ETFC-MPTC is simpler and more practical.

- B. Steady-State Behavior with Anti Load

The ability of three-vector F-ETFC-MPTC and three-vector PI-MPTC-II to resist load torque disturbance is analyzed. Experiments of a sudden increase of a 2 Nm load at a given speed of 300 r/min and a sudden unloading with a 2 Nm load are shown in Figures 17 and 18.

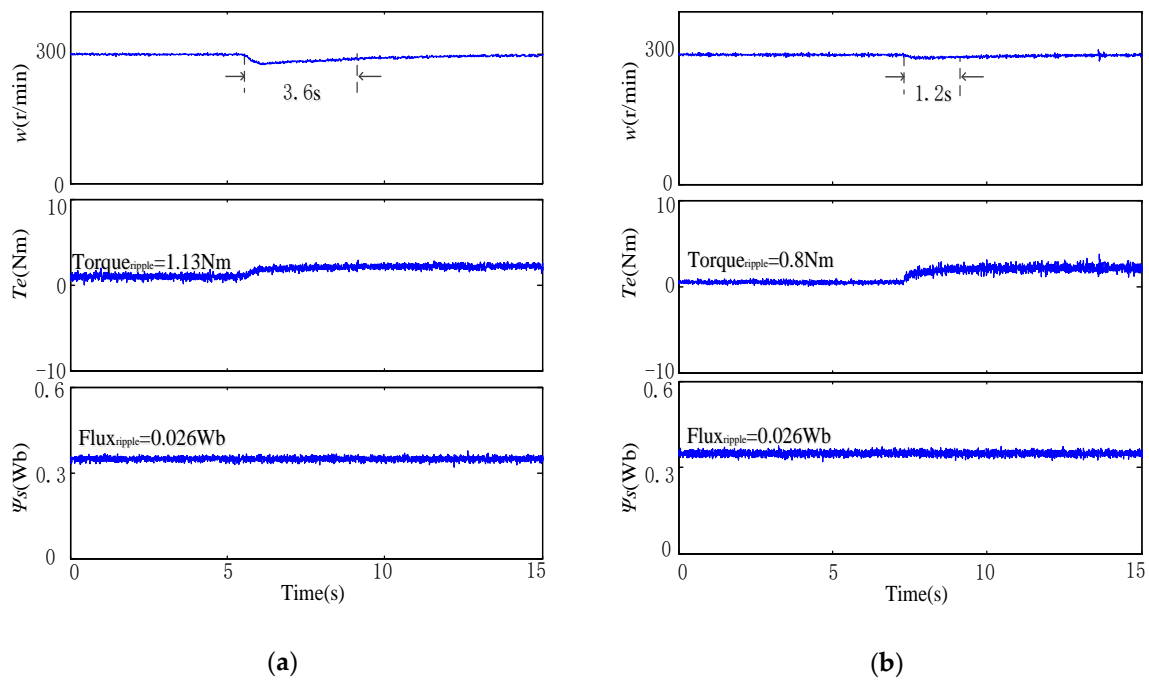


Figure 17. Experimental steady-state waveforms of speed, torque, and stator flux at 300 r/min with a 2 Nm load: (a) PI-MPTC-II, (b) F-ETFC-MPTC.

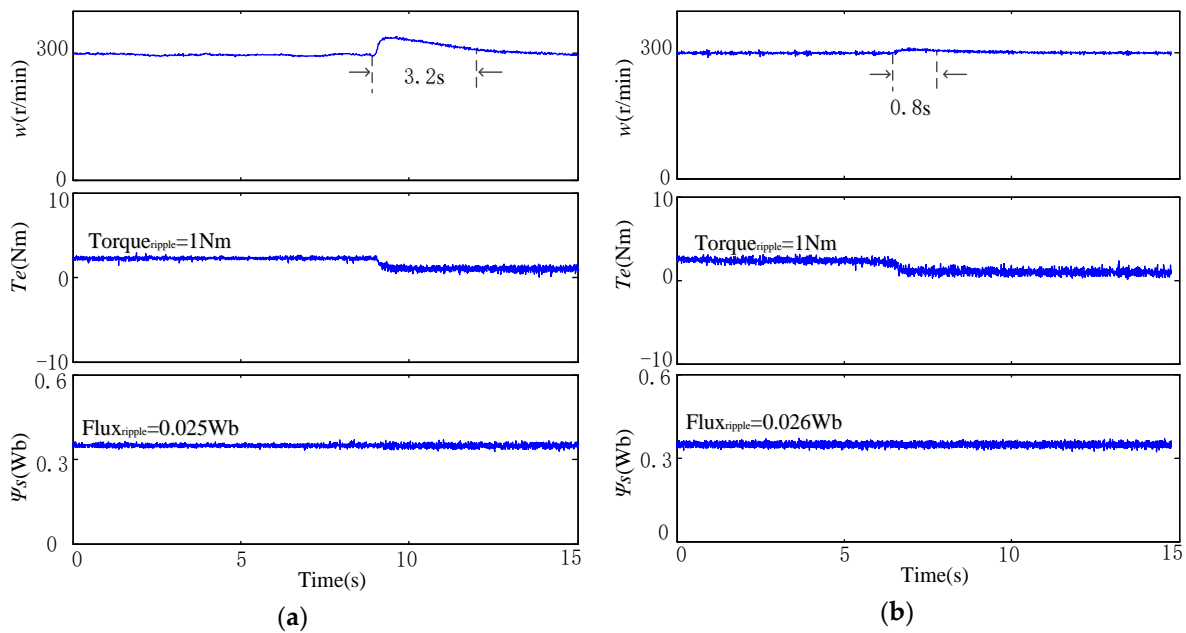


Figure 18. Experimental steady-state waveforms of speed, torque, and stator flux at 300 r/min with a 2 Nm unload: (a) PI-MPTC-II, (b) F-ETFC-MPTC.

It can be seen from the experiment that the flux and torque ripple have little changes in the process of load change, but the value of the flux are kept the same, indicating that the two control strategies are better for the flux and torque decoupling control than others.

When suddenly loaded, according to Figure 17, the stability time of F-ETFC-MPTC is shorter than that of PI-MPTC-II, and the anti-load disturbance ability of the F-ETFC controller is about 66 percent higher than that of the PI controller. In the case of sudden unloading, according to Figure 18, the time taken to reach stability of the F-ETFC-MPTC is also shorter than that of the PI-MPTC-II, and

the anti-load disturbance ability of the F-ETFC controller is about 75 percent higher than that of the PI controller.

- C. Investigation of Average Switching Frequency

Finally, the average switching frequencies of the three methods for different speeds and without loads are presented in Figure 19. From this, it can be seen that the average switching frequencies of PI-MPTC-I noticeably vary over a wide speed range. The switching frequencies of the proposed F-ETFC-MPTC with three vectors is the highest among the three methods, and the average switching frequencies of the PI-MPTC-II are slightly lower. This phenomenon may be caused by the fixed weighting factor in PI-MPTC-II during the whole speed range. This indicates that the three-vector MPTC is more suitable for applications requiring better steady-state behavior, while the single-vector MPTC is more favorable for applications concerning low switching frequency.

Based on the influences of the coaxiality and internal coefficient of friction in the manufacturing process of two motors, no load is equivalent to a certain load, so the electromagnetic torque in the steady state in the experimental waveform is not always zero.

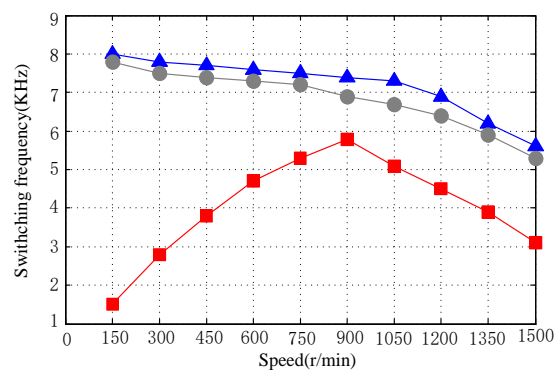


Figure 19. Average switching frequencies for PI-MPTC-I (marked with “□”), PI-MPTC-II (marked with “○”), and F-ETFC-MPTC (marked with “△”) at different speeds without load.

6. Conclusions

Traditional PI-MPTC only applies one voltage vector in each control cycle, which results in a large torque and flux ripple when the speed changes in the traditional MPTC. These restrict the practicability of traditional MPTC. Based on the analysis of model predictive torque control and the combination of PI control strategy and IP control strategy, this paper proposed a F-ETFC speed controller. Compared with the traditional control strategy, it is simpler and more practical, and can effectively improve the anti-load torque disturbance ability and dynamic response of the system.

In the experiment, the motor can restore stability quickly, and the increased electromagnetic torque compensation can improve the anti-load torque disturbance ability of the speed loop by more than 60% and operate normally; and at the same time, the feed-forward factor can realize the optimization of the speed regulation process. It can reduce the adjustment time of the system, increase the speed stability time by more than 10%, and reduce the overshoot of the system. The cost function of the weighted coefficient is replaced by a voltage selection strategy of multi-objective sequencing, which makes F-ETFC-MPTC simpler and more practical. In addition, the improved three-vector algorithm is introduced to improve the steady-state performance, which greatly expands the effective range of the system control set and effectively reduces the flux and torque ripple.

Author Contributions: J.L. and H.L. conceived, designed and performed the algorithm necessary for emulation of the F-ETFC-MPTC, Z.L. designed the hardware, including the DC-AC converter and test-bench system. All authors contributed analysis tools, analysed the data and wrote the paper.

Funding: This research received no external funding.

Conflicts of Interest: The authors declare no conflict of interest.

References

1. Wang, F.; Zhang, Z.; Mei, X.; Kennel, R. Advanced Control Strategies of Induction Machine: Field Oriented Control, Direct Torque Control and Model Predictive Control. *Energies* **2018**, *11*, 120. [[CrossRef](#)]
2. Bermudez, M.; Gonzalez-Prieto, I.; Barrero, F.; Guzman, H.; Duran, M.J.; Kestelyn, X. Open-Phase Fault-Tolerant Direct Torque Control Technique for Five-Phase Induction Motor Drives. *IEEE Trans. Ind. Electron.* **2017**, *64*, 902–911. [[CrossRef](#)]
3. Ahmed, F.I.; El-Tobshy, A.M.; Mahfouz, A.A.; Ibrahim, M.M.S. P-I and I-P controllers in a closed loop for DC motor drives. In Proceedings of the Power Conversion Conference—PCC '97, Nagaoka, Japan, 3–6 August 1997; Volume 2, pp. 613–618.
4. Li, Z.; Zhang, W.; Liu, G.; Wang, B.; Zhang, Y. A novel Integral-Proportional (I-P) speed controller in PMSM motor drive. In Proceedings of the 11th World Congress on Intelligent Control and Automation, Shenyang, China, 29 June–4 July 2014; pp. 4236–4241.
5. Lee, J.H. Model predictive control: Review of the three decades of development[[]]. *Int. J. Control Autom. Syst.* **2011**, *9*, 415. [[CrossRef](#)]
6. Zhao, J.; Quan, X.; Jing, M.; Li, N. Design, Analysis and Model Predictive Control of an Axial Field Switched-Flux Permanent Magnet Machine for Electric Vehicle/Hybrid Electric Vehicle Applications. *Energies* **2018**, *11*, 1859. [[CrossRef](#)]
7. Liu, B.; Chen, T.; Song, W. The essential relationship between deadbeat predictive control and continuous-control-set model predictive control for PWM converters. In Proceedings of the 2018 International Power Electronics Conference (IPEC-Niigata 2018-ECCE Asia), Niigata, Japan, 20–24 May 2018; pp. 1872–1876.
8. Chen, Z.; Qiu, J.; Mengjia, J. Prediction-Error-Driven Position Estimation Method for Finite-Control-Set Model Predictive Control of Interior Permanent-Magnet Synchronous Motors. *IEEE J. Emerg. Sel. Top. Power Electron.* **2019**, *7*, 282–295. [[CrossRef](#)]
9. Xu, Y.; Zhang, B.; Zhou, Q. A model predictive current control method of PMSM based on the simultaneous optimization of voltage vector and duty cycle. In Proceedings of the 2016 IEEE 8th International Power Electronics and Motion Control Conference (IPEMC-ECCE Asia), Hefei, China, 22–26 May 2016; pp. 881–884.
10. Aciego, J.J.; Gonzalez Prieto, I.; Duran, M.J. Model Predictive Control of Six-Phase Induction Motor Drives Using Two Virtual Voltage Vectors. *IEEE J. Emerg. Sel. Top. Power Electron.* **2019**, *7*, 321–330. [[CrossRef](#)]
11. Geyer, T.; Papafotiou, G.; Morari, M. Model Predictive Direct Torque Control—Part I: Concept, Algorithm, and Analysis. *IEEE Trans. Ind. Electron.* **2009**, *56*, 1894–1905. [[CrossRef](#)]
12. Davari, S.A.; Khaburi, D.A.; Stolze, P.; Kennel, R. An improved Finite Control Set-Model Predictive Control (FCS-MPC) algorithm with imposed optimized weighting factor. In Proceedings of the 2011 14th European Conference on Power Electronics and Applications, Birmingham, UK, 30 August–1 September 2011; pp. 1–10.
13. Xiao, M.; Yan, Y.; Xu, W.; Shi, T.; Xia, C. Torque control of permanent magnet synchronous motor using flux vector. In Proceedings of the 2017 20th International Conference on Electrical Machines and Systems (ICEMS), Sydney, Australia, 1–14 August 2017; pp. 1–5.
14. Zhang, X.; He, Y.; Hou, B. Double Vector Based Model Predictive Torque Control for SPMSM Drives with Improved Steady-State Performance. *J. J. Power Electron.* **2018**, *18*, 1398–1408.
15. Changliang, X.; Xudong, Q.; Zhiqiang, W.; Tingna, S. Predictive Torque Control Based on Optimal Operating Time of Vector. *J. Chin. J. Electr. Eng.* **2016**, *36*, 3045–3053.
16. Hassine, I.M.; Naouar, M.W.; Mrabet-Bellaaj, N. Model Predictive-Sliding Mode Control for Three-Phase Grid-Connected Converters. *IEEE Trans. Ind. Electron.* **2017**, *64*, 1341–1349. [[CrossRef](#)]
17. Zhang, Y.; Xie, W.; Li, Z.; Zhang, Y. Low-Complexity Model Predictive Power Control: Double-Vector-Based Approach. *IEEE Trans. Ind. Electron.* **2014**, *61*, 5871–5880. [[CrossRef](#)]
18. Zhang, Y.; Yang, H. Generalized Two-Vector-Based Model-Predictive Torque Control of Induction Motor Drives. *IEEE Trans. Power Electron.* **2015**, *30*, 3818–3829. [[CrossRef](#)]
19. Zhang, Y.; Yang, H. Two-Vector-Based Model Predictive Torque Control Without Weighting Factors for Induction Motor Drives. *IEEE Trans. Power Electron.* **2016**, *31*, 1381–1390. [[CrossRef](#)]
20. Zhang, Y.; Xia, B.; Yang, H. A novel three-vectors-based model predictive flux control of induction motor drives. In Proceedings of the 2016 IEEE 8th International Power Electronics and Motion Control Conference (IPEMC-ECCE Asia), Hefei, China, 22–26 May 2016; pp. 367–373.

21. Rojas, C.A.; Rodriguez, J.; Villarroel, F.; Espinoza, J.R.; Silva, C.A.; Trincado, M. Predictive Torque and Flux Control Without Weighting Factors. *IEEE Trans. Ind. Electron.* **2013**, *60*, 681–690. [[CrossRef](#)]
22. Rodriguez, J.; Kennel, R.M.; Espinoza, J.R.; Trincado, M.; Silva, C.A.; Rojas, C.A. High-Performance Control Strategies for Electrical Drives: An Experimental Assessment. *IEEE Trans. Ind. Electron.* **2012**, *59*, 812–820. [[CrossRef](#)]
23. Vyncke, T.J.; Thielemans, S.; Dierickx, T.; Dewitte, R.; Jaxsens, M.; Melkebeek, J.A. Design choices for the prediction and optimization stage of finite-set model based predictive control. In Proceedings of the 2011 Workshop on Predictive Control of Electrical Drives and Power Electronics, Munich, Germany, 14–15 October 2011; pp. 47–54.



© 2019 by the authors. Licensee MDPI, Basel, Switzerland. This article is an open access article distributed under the terms and conditions of the Creative Commons Attribution (CC BY) license (<http://creativecommons.org/licenses/by/4.0/>).